Journal of Achievements in Materials and Manufacturing Engineering
VOLUME 34
ISSUE 1
May
2009

Structure investigation of the Al-Si-Cu alloy using derivative thermo analysis

M. Krupiński*, K. Labisz, L.A. Dobrzański
Division of Materials Processing Technology, Management and Computer Techniques in Materials Science, Institute of Engineering Materials and Biomaterials, Silesian University of Technology, ul. Konarskiego 18a, 44-100 Gliwice, Poland
* Corresponding author: E-mail address: mariusz.krupinski@polsl.pl

Received 12.02.2009; published in revised form 01.05.2009

Properties

ABSTRACT

Purpose: This research work presents the investigation results of derivative thermoanalysis performed using the UMSA device (Universal Metallurgical Simulator and Analyzer). The material used for investigation was an Al-Si-Cu alloy known as AC-AlSi7Cu3Mg grade aluminium cast alloy.
Design/methodology/approach: As a result of this research the cooling rate influence on structure and mechanical properties changes, especially HB Hardness was investigated. The cooling rate was set in a variable range of ~0.2 ºC/s to ~1.25 ºC/s. In this work structure changes were determined concerning the structure, especially the dendrites and grains and particle distribution in the aluminium matrix.
Findings: The reason of this work was to determine the optimal cooling rate values, to achieve good mechanical properties for protection of this aluminium cast alloy from losing their work stability and to make it more resistant to action in hard working conditions. For investigations of the aluminium samples hardness measurements of the different sample areas were performed. The material was examined metallographically and analyzed qualitatively using light and scanning electron microscope as well as the area mapping and point-wise EDS microanalysis. The performed investigation are discussed for the reason of an possible improvement of thermal and structural properties of the alloy. The investigation revealed the formation of aluminium reach (α -Al) dendrites and also the occurrence of the α+β eutectic, the ternary eutectic α+Al_2Cu+β, as well the occurrence of the Fe and Mn containing phase was confirmed.
Practical implications: In the metal casting industry, an improvement of component quality depends mainly on better control over the production parameters.
Originality/value: This work provides also a better understanding of the thermal characteristics and processes occurred in the new developed near eutectic Al–Si-Cu alloy. The achieved results can be used for liquid metal processing in science and industry and obtaining of a required alloy microstructure and properties influenced by a proper production conditions.
Keywords: Aluminium alloys; Mechanical properties; Thermo analysis; Structure; UMSA

Reference to this paper should be given in the following way:
M. Krupiński, K. Labisz, L.A. Dobrzański, Structure investigation of the Al-Si-Cu alloy using derivative thermo analysis, Journal of Achievements in Materials and Manufacturing Engineering 34/1 (2009) 47-54.

1. Introduction

Aluminium alloys are especially preferred in designs thanks to their good mechanical properties and possibility to make very complicated castings with high service properties. Thanks to the contemporary casting and heat treatment technologies, castings from the aluminium alloys have the suitably high mechanical properties and simultaneously decrease the part weight.

Therefore, there are more and more frequently used in the means of transport industry [1-5].

These alloys have become popular in automotive industry owing to their low weight and some casting and mechanical qualities. The main component of aluminum alloy casting is Si. The eutectic structure in Al-Si cast alloys and Si concentration largely affect the porosity (pore volume) [6].

In recent years together with the development of the car industry and the desire for lowering the energy consumption of production processes, tendencies have appeared to return to casting alloys in sand moulds made on highly efficient automatic lines. The examples of using such solutions can be very often used technologies like Cosworth, CPS, BAXI and HWS. These technologies ensure filling the sand moulds with the elevated pressure and reduce oxidation of the applied aluminum alloys. The usage of highly efficient automatic cast lines has made it necessary to work out a fast, cheap and precise estimation method of the quality of cast alloys [2].

The modification of Al alloys causes relatively the biggest difficulties. It is common knowledge that the modification of alloys influences the number of nuclei in terms of their decrease, increase or passivation. Harmful elements, in turn, cause the cast porosity, lowering significantly their mechanical properties [7].

Change of crystallization kinetic is caused by appliance of different cooling rate and influences the crystallization overcooling grade of the α solid solution, $\alpha+\beta$ eutectic, this can be state in the microstructure and that fore also in the change of the mechanical properties of the Al–Si–Cu aluminium cast alloys. Exact knowledge of the cooling rate influence of the Sand casts on structure and temperature of the phase transformations during non-equilibrium crystallization allows to perform an optimization of the production process. The above mentioned premises makes it possible to state, that the actually studying subject matter concerning crystallization kinetics of the Al–Si–Cu aluminium cast alloys, can be considered as up-to-date not only because of the scientifically point of view, but also for the reason of practically application of the elaborated results.

Parameters describing the crystallization kinetics are variables of crystallization time and geometrical coordinates of the cast.

A complete characterization of the crystallization kinetics is achieved after coupling of crystallization equation with heat transport equation, where the emitted crystallization heat is considered as a factor which combines this two equation together and depends on the fraction of the crystallized structure components.

Crystallization of the liquid alloy is going from the liquid state to the liquidus line, that is to the beginning of the crystallization, after that follows crystallization of the eutectics and intermetallic phases to the point where the alloy is solid – the solidus line according to the equilibrium diagrams [8-13].

For this reason on the crystallization curie occurs some characteristic inflexion points coming from exothermic or endothermic reactions of the crystallizing phase transformations. It is difficult to determine unequivocally the crystallization temperature of the phases occurred on the crystallization curve. The determination is possible using the first derivative curve of the cooling line in function of time, that mines using the differential ATD curve called also derivative curve.

When crystallization heat is emitted, that means when crystallization proceeds, the momentary heat effect id described by the following interdependence:

$$\frac{dQ}{dt} = c_p(t) \cdot m \cdot \left[\frac{dT}{dt} - \left(\frac{dT}{dt} \right)_b \right] \tag{1}$$

Calculating the crystallisation heat effect at the time t it is necessary to take into account also the heat capacity, which depends on the ratio of the crystallised material land the remained liquid metal. Heat capacity as a function of t is characterised by the following equation:

$$c_p(t) = c_{p_{Sol}} \cdot \int_{t_N}^{t} f_S(t)dt + c_{p_{Liq}} \cdot \left(1 - \int_{t_N}^{t} f_S(t)dt \right) \tag{2}$$

Total crystallisation heat can be calculated using an integral of the following equation (2):

$$Q = c_p \cdot m \cdot \int_{t_N}^{t_{Sol}} \left[\frac{dT}{dt} - \left(\frac{dT}{dt} \right)_b \right] dt \tag{3}$$

The general equation, describing (Table 1) the crystallisation function as a derivative of the crystallisation, is given as:

$$\frac{dT}{dt} = \frac{A}{m \cdot c_p} \cdot \alpha(t) \cdot (T - T_0) + \frac{K_K}{m \cdot c_p} \cdot \left(m \frac{dz}{dt} + z \frac{dm}{dt} \right) \tag{4}$$

In the time without any phase transformations, that means any other heat sources are not present, the differentia curie covers the base line [6, 14, 15].

Table 1.
Description of the equation factors

Symbol	Descriptions
Q	Crystallisation heat
cp	Heat capacity
m	Mass of the crystallised metal
f_S	Ratio of the solid fraction
$\alpha(T)$	Heat transport coefficient through the sampler
T	Temperature at time dt
T_O	Environment temperature
A	Sampler surface
K_K	Crystallisation constant
z	Nucleus number

The UMSA device used for investigations is designed to overcome the existing problem of laboratory and industrial equipment on the present market. This platform combines computer controlled melting and heat treatment devices with a quench equipment, as well the device for thermal analysis and testing equipment for in-situ investigations of test sample crystallization characteristics.

The UMSA device is used mostly in the following areas:

- development of new materials and processes as well in quality control process,
- analysis of phase nucleation, crystallization and growth, phase transformations during melting, solidification,
- heat treatment performed under assumed conditions,
- physical simulation of metal casting technologies including melting, chemical and thermal treatment, solidification and heat treatment operations with operations like solution heat treatment, aging and quenching,
- analysis of structure changes of the test sample material according to quenching at determined temperatures [16].

2. Materials and experimental procedure

For statement of the interdependence between the chemical composition and the structure of the AC-AlSi7Cu3Mg (EN 1706:2001) aluminium cast alloy (Table 2), cooled with different cooling speed, followed investigations were made:

- Alloy structure using MEF4A optical microscope supplied by Leica together with the image analysis software as well electron scanning microscope using Zeiss Supra 25 device within high resolution mode. The samples for optical microscope investigations were electro etched using 30% HBF_4 solution with proper direct current conditions as well in the 5% HF solution.
- phase composition using EBSD and chemical composition of the Al alloy using qualitative and quantitative X-Ray analysis, as well EDS microanalysis,
- derivative thermo analysis using the UMSA thermo simulator (Fig. 1),
- hardness was measured using the Rockwell hardness tester supplied by Zwick ZHR 4150.

Table 2.
Chemical composition of AC-AlSi7Cu3Mg aluminum alloy

Mass concentration of the element, in wt. %, AA standard			
Si	Cu	Mg	Mn
6.5-8	3-4	0.3-0.6	0.2-0.65
Fe	Ti	Zn	Ni
≤ 0.8	≤ 0.25	≤ 0.65	≤ 0.3

Material used for investigations was cut from the car engine block cast.

Heating system scheme with placed sample was presented on Fig. 2. The figure shows the cylindrical sample used for investigation of the B –type, form cylindrical samples of the A type without the cooling pipe in the center of the sample, the second thermocouple is placed in the sample axis.

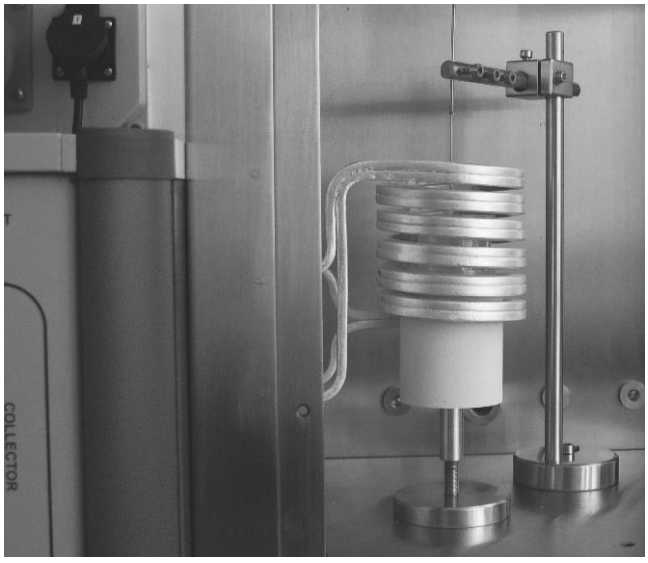

Fig. 1. View of the sample placed in the UMSA device

Diameter dimensions used in the performed investigations are showed on Fig. 3. For sample cooling compressed air gas was used, and the cooling rate was defined as temperature decrease pre time in the solidus - liquidus range.

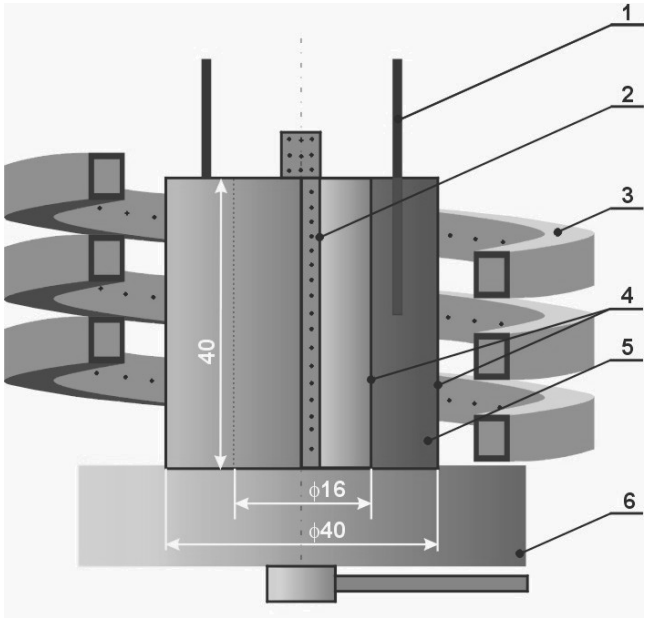

Fig. 2. Heating and cooling system scheme of the UMSA device, thermocouples placement and samples dimensions, for cylindrical sample of the B type: 1- thermocouple, 2- cooling pipe, 3- induction coil, 4- cooling nozzles, 5 – sample, 6 – sample isolation

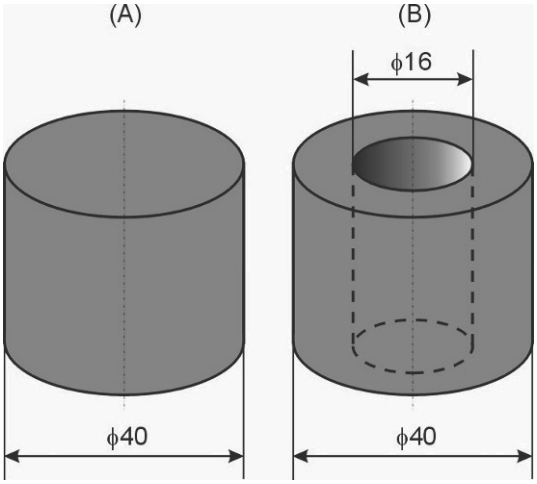

Fig. 3. Dimensions of the cylindrical sample types used for investigations

For measurement and recording of the temperature changes a K-type (chromo–alumel) thermocouples was used. Tests were performed several times for each cooling speed for statistical estimation of the investigation results.

3. Results and discussion

As a result of the phase and chemical composition investigations of the Al no changes in the phase composition of the Al grade cast alloy were detected caused by different cooling rates. Changes in the cooling rate influence the morphology of the precipitations present in the investigated alloys, particularly on the morphology of the β phase. Cooling speed of the investigated Al Alloy samples causes the structure refinement (Figs. 4-11) as well as morphology change of the phases, that confirms also investigations using light microscope.

On the basis of the performed quantitative microanalysis, using the EDS microanalysis method, information was achieved about the mass and atomic concentration of particular elements in the point-wise analyzed areas of the matrix as well the precipitations (Figs. 13-17). Investigations using the scanning electron microscope revealed, that the phases of the Al alloy consist mainly of the following elements: Al, Cu, Fe, Mn, Si and Mg. Microstructure investigations carried out using the electron scanning microscope and quantitative X-Ray analysis confirms the occurrence of the α+β eutectic (Fig. 12) in the investigated alloy, and allows to assume, that in the investigated alloy also the triple eutectics $\alpha+Al_2Cu+\beta$ are present, moreover in the investigated alloys there are also complex multicomponent eutectics, probably of the $\alpha+Al_2Cu+AlSiMgCu+\beta$ type as well the Al+Fe+Mn+Si phase are present.

Change of the cooling rate of the investigated alloy in the range of 0.2°C/s to ~1.25°C/s causes a hardness increase from 69 HB for the 0.2°C/s cooling rat to 92 HB for the 1.25°C/s cooling rate (Fig. 19).

Representative cooling and crystallisation curves of the investigated cast Al–Si–Cu alloys, cooled with different cooling rates are presented on Figure 20. Analyzing the crystallisation process on the basis of the cooling curves is was state that at the T_{DN} temperature starts the nucleation process of the α phase dendrites. On the derivative curve it is visible as a small inflexion point marked as *I*, as well a temporary decrease in the cooling rate of the alloy. Heat effect accomplished to the nucleation process provide additionally heat to the remaining melt, however heat balance of the crystllised ingot is negative. The heat provided by the nuclei of the α phase is disproportional smaller compared to the heat give up to the surrounding through the cooled metal and causes only cooling rate decrease of the remaining melt. This process is going until the minimum of the crystallisation temperature of the dendrite α phase (point *II* in the curve) is achieved, where the created nuclei achieves the critical value and the growing process of the α phase dendrite crystals is beginning.

The differential curve in this point takes zero as value. The crystallisation heat warms up the remaining melt to the temperature at point *III*, where the created and freely growing crystals of the dendritic α phase begin to touch each others with some surfaces include the remaining melt inside. Next growth of the crystals causes a temperature increase of the melt to the maximal temperature value of the crystllised α phase, (point *IV*), at this moment also the Al+Fe+Mn+Si phase crystallisation occurs, what is confirmed in the literature [14, 15]. The chemical composition of the remained melt changes according to the liquidus line in the Al–Si equilibrium diagram. The melt is enriched with Si and after the temperature At point *V* is achieved the nucleation of the α+β eutectic begins. The temperature grows to the maximal crystallisation temperature of the eutectic (point *VII*), where the spontaneous precipitation of the durable α i β phases occurs. Next undercooling of the melt causes the crystallisation of the Cu and Mg reach phases, which emit additive crystallisation heat, this is shown on the differential curve in form of clearly heat effects (point *VIII* and *IX*). The crystallisation ends after the T_{Sol} solidus temperature is achieved (point *X*). In Table 3 the characteristic points of the cooling curie are described.

Table. 3.
Description of the characteristic points on the cooling curie from Fig. 20

Point on the graph	Description
I	T_{DN} nucleation temperature
II	T temperature of the beginning of the crystal growth (α phase dendrites)
III	Dendrites (α phase) growth temperature
IV	Temperature of α phase dendrite growth and (Al+Fe+Mn+Si) precipitation growth
V	Nucleation temperature of the α+βeutectics
VI	Temperature of the α+β eutectics growth
VII	Temperature of the stable eutectic growth α+β, in this point occurs the thermal equilibrium of the crystallized phases
VIII	Crystallization temperature of Cu phase and α+β eutectic
IX	Crystallization temperature of Mg, Cu phase and α+β eutectic
X	T_{Sol} temperature of the crystallization end

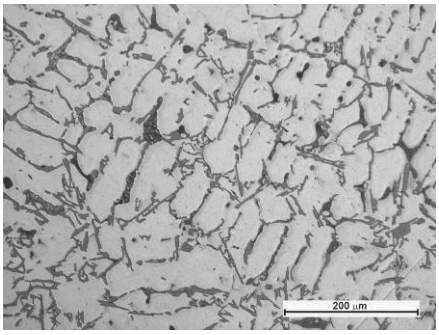

Fig. 4. Optical micrograph of the Al alloy, cylindrical sample of the A type, cooling rate 1.25°C/s, plane perpendicular to the sample axis

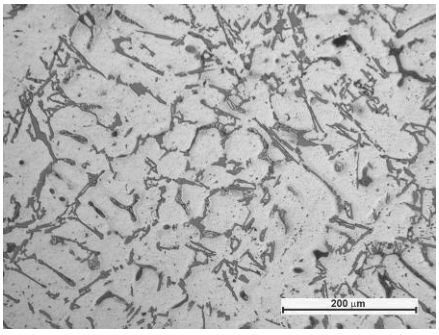

Fig. 5. Optical micrograph of the Al alloy, cylindrical sample of the B type, cooling rate 1°C/s, plane perpendicular to the sample axis

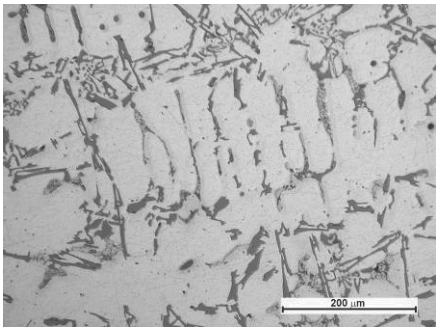

Fig. 6. Optical micrograph of the Al alloy, cylindrical sample of the A type, cooling rate 0.5°C/s, plane perpendicular to the sample axis

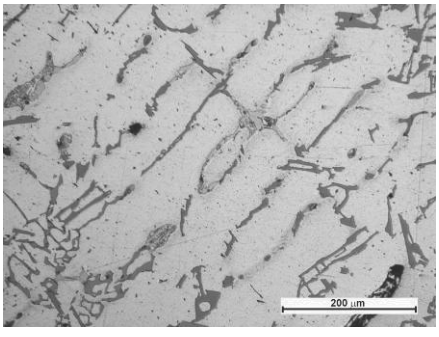

Fig. 7. Optical micrograph of the Al alloy, cylindrical sample of the A type, cooling rate 0.2°C/s, plane perpendicular to the sample axis

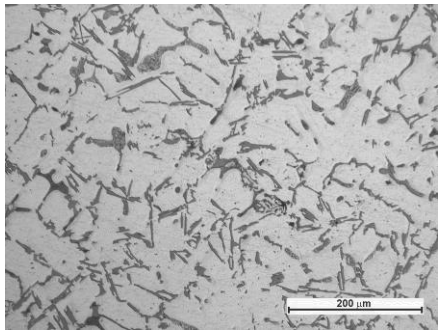

Fig. 8. Optical micrograph of the Al alloy, cylindrical sample of the A type, cooling rate 1.25°C/s, plane parallel to the sample axis

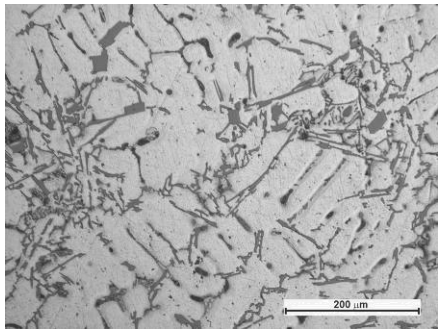

Fig. 9. Optical micrograph of the Al alloy, cylindrical sample of the B type, cooling rate 1°C/s, plane parallel to the sample axis

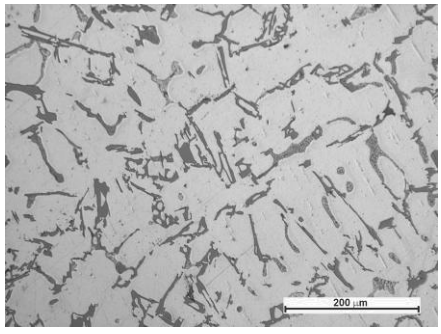

Fig. 10. Optical micrograph of the Al alloy, cylindrical sample of the A type, cooling rate 0.5°C/s, plane parallel to the sample axis

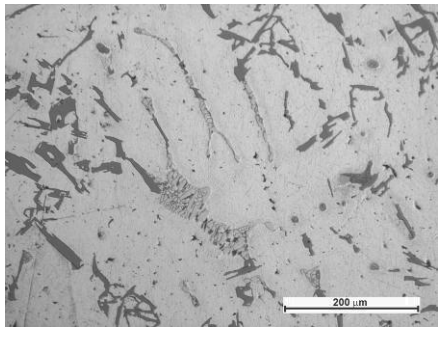

Fig. 11. Optical micrograph of the Al alloy, cylindrical sample of the A type, cooling rate 0.2°C/s, plane parallel to the sample axis

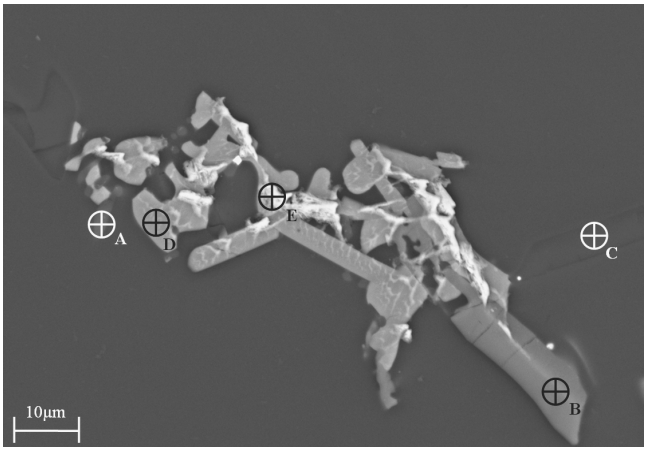

Fig. 12. SEM micrograph of the investigated Al alloy

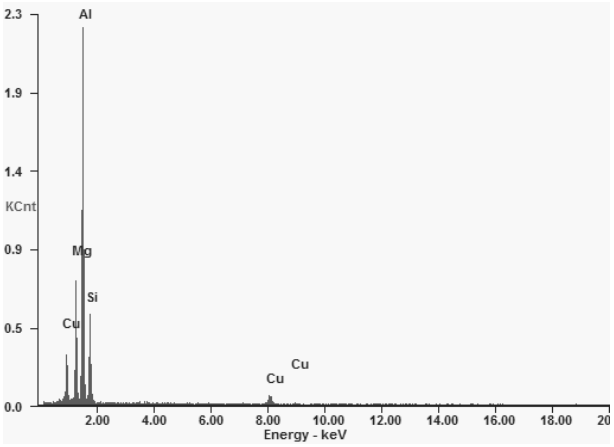

Fig. 13. EDS point wise analysis of the investigated aluminium cast alloy, marker A in Figure 12

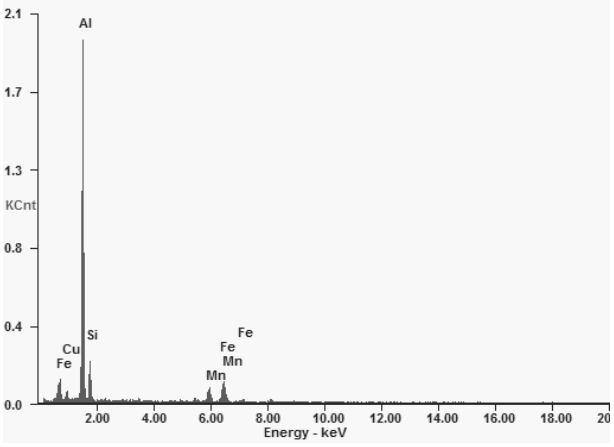

Fig. 14. EDS point wise analysis of the investigated aluminium cast alloy, marker B in Figure 12

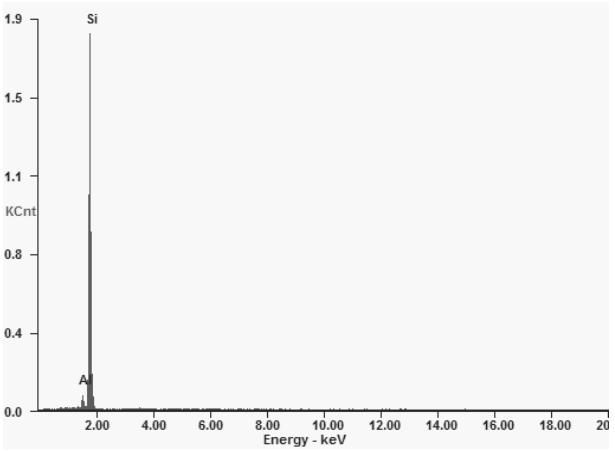

Fig. 15. EDS point wise analysis of the investigated aluminium cast alloy, marker C in Figure 12

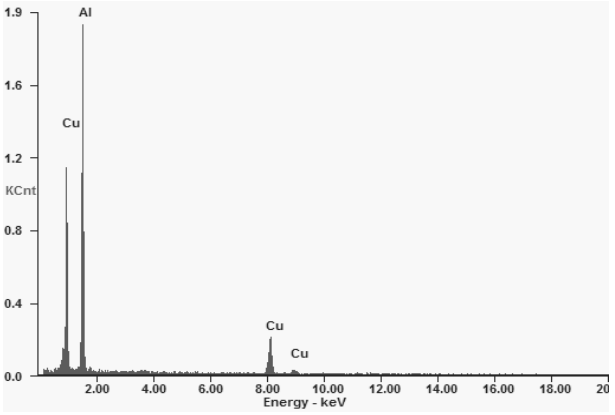

Fig. 16. EDS point wise analysis of the investigated aluminium cast alloy, marker D in Figure 12

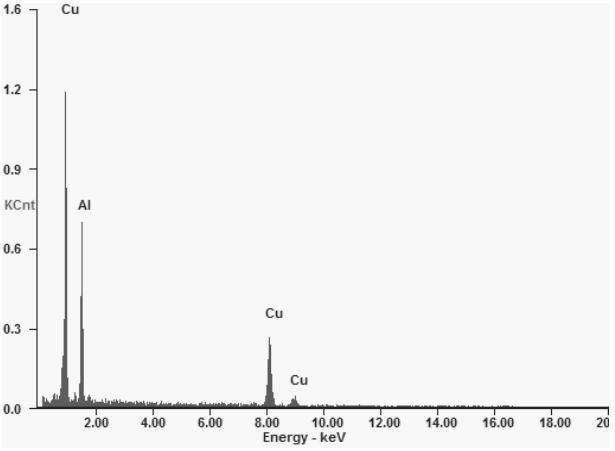

Fig. 17. EDS point wise analysis of the investigated aluminium cast alloy, marker E in Figure 12

As a result of the EDS chemical composition of the investigated phase, presented on Figs. 12 and 13, the presence of Al, Cu, Mg and Si was confirmed. On the basis of the EBSD investigation the occurrence of the $Cu_{3,84}Mg_2Si_{0,96}$ phase was confirmed (Fig. 18). The presence of Al in the EDS results is probable caused by Al matrix influence. Next investigations for $Cu_{3,84}Mg_2Si_{0,96}$ phase identification will be performed mainly using diffraction method on transmission electron microscope.

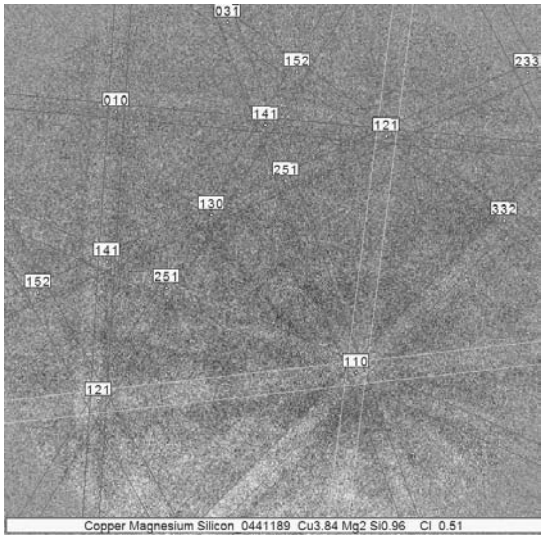

Fig. 18. EBSD analysis result

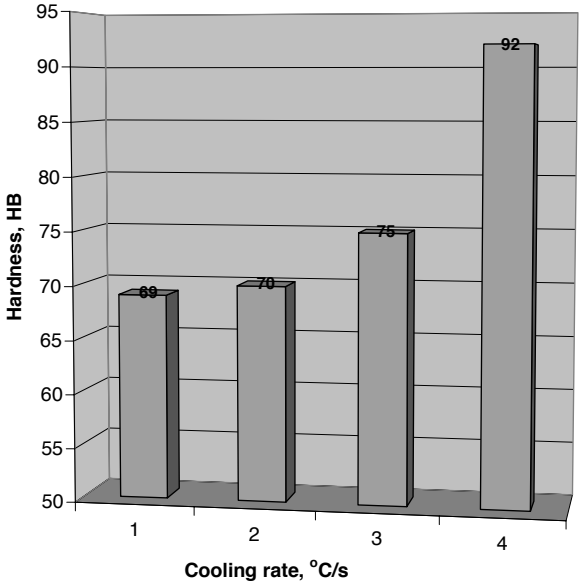

1 – cylindrical sample of type A, cooling rate 0.2°C/s
2 – cylindrical sample of type A, cooling rate 0.5°C/s
3 – cylindrical sample of type A, cooling rate 1°C/s
4 – cylindrical sample of type B, cooling rate 1.25°C/s

Fig. 19. Diagram of the dependence of hardness values on cooling rate

a)

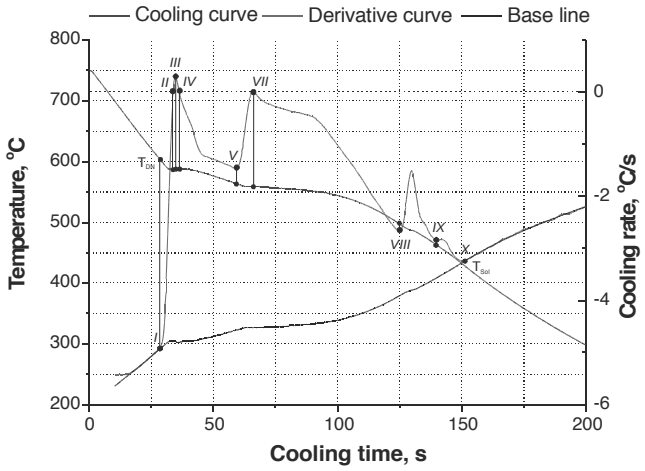

b)

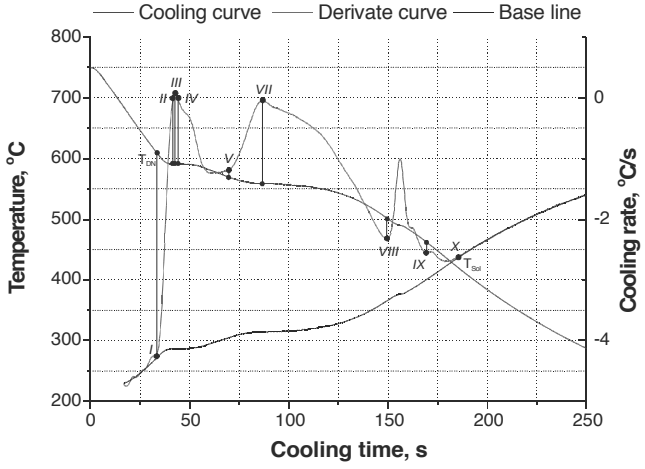

c)

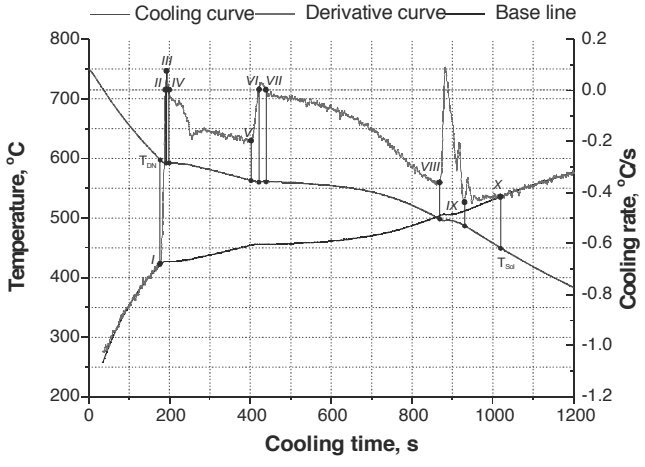

Fig. 20. Cooling curve, crystallisation curve and baseline of the AC-AlSi7Cu3Mg alloy cooled with different cooling rate: a) 1.25°C/s, b) 1°C/s, c) 0.2°C/s

4. Conclusions

Changes in the cooling rate causes modifications of the phase morphology and shape and as a consequence, effect the structure refinement. Increase of the cooling rate causes also an moderate hardness increase of the investigated Al-Si-Cu samples, the measure hardness values increases form 69 HB for the lowest cooling rate to 92 HB for the highest applied cooling rate value.

Cooling rate change in the range of 0.2 to 1.25°C/s does not influence the chemical composition of the phases occurred in the investigated alloy, which was confirmed using the EDS analysis. As a result of the EBSD investigation the Cu+Mg+Si phase occurrence was confirmed in the Al alloy.

References

[1] L.A. Dobrzański, K. Labisz, A. Olsen, Microstructure and mechanical properties of the Al-Ti alloy with calcium addition, Journal of Achievements in Materials and Manufacturing Engineering 26/2 (2008) 183-186.

[2] K.W. Dolan, Design and Product Optimization for Cast Light Metals, 2000, Livermore.

[3] M. Panušková, E. Tillová, M. Chalupová, Relation between mechanical properties and microstructure of cast aluminum alloy AlSi9Cu3, Strength of Materials 40/1 (2008) 98-101.

[4] F.J. Tavitas-Medrano, J.E. Gruzleski, F.H. Samuel, S. Valtierra, H.W. Doty, Effect of Mg and Sr-modification on the mechanical properties of 319-type aluminum cast alloys subjected to artificial aging, Materials Science & Engineering A 480/1-2 (2008) 356-364.

[5] Q.G. Wang, Microstructural effects on the tensile and fracture behavior of aluminum casting alloys A356/357, Metallurgical and Materials Transactions A 34/12 (2003) 2887-2899.

[6] L.A. Dobrzański, R. Maniara, J.H. Sokolowski, The effect of cast Al-Si-Cu alloy solidification rate on alloy thermal characteristics, Journal of Achievements in Materials and Manufacturing Engineering 17 (2006) 217-220.

[7] L.A. Dobrzański, R. Maniara, J.H. Sokolowski, W. Kasprzak, M. Krupiński, Z. Brytan, Applications of the artificial intelligence methods for modeling of the ACAlSi7Cu alloy crystallization process, Journal of Materials Processing Technology 192-193 (2007) 582-587.

[8] M.J. Caton, J. Jones, Wayne, J.M. Boileau, J.E. Allison, The effect of solidification rate on the growth of small fatigue cracks in a cast 319-type aluminum alloy, Metallurgical and Materials Transactions A 30/12 (1999) 3055-3068.

[9] M.I. Hussain, K.S. Taraman, A.J. Filipovic, I. Garrn, Experimental study to analyse the workpiece surface temperature in deep hole drilling of aluminium alloy engine blocks using MQL technology, Journal of Achievements in Materials and Manufacturing Engineering 31/2 (2008) 485-490.

[10] F.C. Robles Hernandez, M.B. Djurdjevic, W.T. Kierkus, J.H. Sokolowski, Calculation of the liquidus temperature for hypo and hypereutectic aluminum silicon alloys, Materials Science and Engineering A 396 (2005) 271-276.

[11] J. Szajnar, T. Wróbel, Methods of inoculation of pure aluminium structure, Journal of Achievements in Materials and Manufacturing Engineering 27/1 (2008) 95-98.

[12] H. Yamagata, W. Kasprzak, M. Aniolek, H. Kurita, J.H. Sokolowski, The effect of average cooling rates on the microstructure of the Al–20% Si high pressure die casting alloy used for monolithic cylinder blocks, Journal of Materials Processing Technology 203 (2008) 333-341.

[13] H. Yamagata, H. Kurita, M. Aniolek, W. Kasprzak, J.H. Sokolowski, Thermal and metallographic characteristics of the Al–20% Si high-pressure die-casting alloy for monolithic cylinder blocks, Journal of Materials Processing Technology 199 (2008) 84-90.

[14] L. Bäckerud, G. Chai, J. Tamminen, Solidification Characteristics of Aluminum Alloys, Vol. 2, AFS, 1992.

[15] L. Bäckerud, G. Chai, Solidification Characteristics of Aluminum Alloys, Vol. 3, AFS, 1992.

[16] L.A. Dobrzański, W. Kasprzak, M. Kasprzak, J.H. Sokolowski, A novel approach to the design and optimization of aluminum cast component heat treatment processes using advanced UMSA physical simulations, Journal of Achievements in Materials and Manufacturing Engineering 24/2 (2007) 139-142.